A Signal-Space Analysis of Spatial Self-Interference Isolation for Full-Duplex Wireless

Evan Everett
Rice University

Ashutosh Sabharwal
Rice University

***Abstract*—The challenge to in-band full-duplex wireless communication is managing self-interference. Many designs have employed spatial isolation mechanisms, such as shielding or multi-antenna beamforming, to isolate the self-interference wave from the receiver. Such spatial isolation methods are effective, but by confining the transmit and receive signals to a subset of the available space, the full spatial resources of the channel be under-utilized, expending a cost that may nullify the net benefit of operating in full-duplex mode. In this paper we leverage an antenna-theory-based channel model to analyze the spatial degrees of freedom available to a full-duplex capable base station, and observe that whether or not spatial isolation out-performs time-division (i.e. half-duplex) depends heavily on the geometric distribution of scatterers. Unless the angular spread of the objects that scatter to the intended users is overlapped by the spread of objects that backscatter to the base station, then spatial isolation outperforms time division, otherwise time division may be optimal.**

I. Introduction

Consider the communication scenario depicted in Figure 1. User 1 wishes to transmit uplink data to a base station, and User 2 wishes to receive downlink data from the same base station. If the base station can operate in full-duplex mode, i.e., transmits and receives at the same time in the same band, then it can enhance spectral efficiency by servicing both users simultaneously. To cancel the high-powered self-interference, the knowledge of the transmit signal can be used to perform self-interference cancellation. However, experimental studies have shown that cancellation alone is often insufficient to realize the ideal doubling of capacity over half-duplex [1], [2]. Thus methods to create spatial isolation between transmit and receive antennas, like multi-antenna beamforming [3], [4], directional antennas [5], and shielding via absorptive materials [6], are also employed. Unlike cancellation, spatial isolation may consume channel resources that could have otherwise been leveraged for signal-of-interest communication.

Consider the example illustrated in Figure 1. The direct path from the base station transmitter, T_2, to its receiver R_1, can be suppressed by creating a radiation pattern with a null in the direction of R_1, but there will also be self-interference due to reflections from the scatterers. The self-interference caused by scatterer S_0 in Figure 1 could be avoided by creating a null in the direction of S_0. However losing access to that scatterer could lead to a less rich scattering environment, diminishing the spatial degrees of freedom of the uplink or downlink.

Question: Under what scattering conditions can spatial isolation be leveraged to provide a degree-of-freedom gain over half duplex? More specifically, given a constraint on the *area* of the arrays at the base station and at the User 1 and User 2 devices, and given a characterization of the *spatial distribution* of the scatterers in the environment, what is the uplink/downlink degree-of-freedom region when the only self-interference mitigation strategy is spatial isolation?

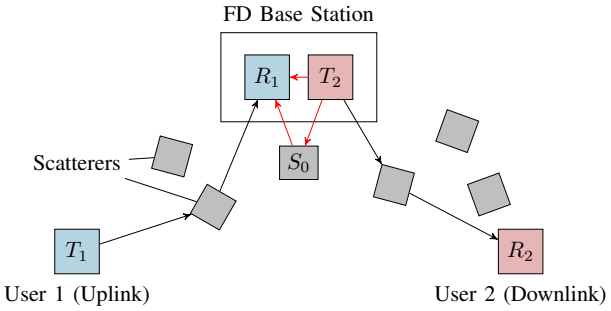

Fig. 1: Three-node full-duplex model

Modeling Approach: To answer the above question we leverage physical channel model developed by Poon, Brodersson, and Tse in [7]–[9], which we will call the "PBT" model. In the PBT model, instead of constraining the *number* of antennas, a constraint on the *area* of the array is given, and instead of considering a channel matrix drawn from a probability distribution, a channel transfer function which depend on the geometric position of the scatterers relative to the arrays is considered.

Contribution We extend the PBT model to the three-node full-duplex topology of Figure 1, and derive the degree-of-freedom region $\mathcal{D}_{\mathsf{FD}}$, i.e. the set of all achievable uplink/downlink degree-of-freedom tuples. By comparing $\mathcal{D}_{\mathsf{FD}}$ to $\mathcal{D}_{\mathsf{HD}}$, the degree-of-freedom region achieved by time-division duplex, we observe that $\mathcal{D}_{\mathsf{HD}} \subset \mathcal{D}_{\mathsf{FD}}$ in the following two scenarios:

1) When the base station arrays are larger than the corresponding user arrays, so that the extra resources used for spatial isolation were not needs for spatial multiplexing,
2) More interestingly, when the forward scattering intervals and the backscattering intervals are not completely overlapped. In Figure 1 for example, if there are some directions from which T_2's radiated signal will scatter to the intended receiver, R_2, but not backscatter to R_1, then T_2 can avoid interference by signaling in those directions

without having to zero-force to R_2.

II. System Model

Here we extend the PBT channel model in [7], which considers a point-to-point topology, to the three-node full-duplex topology of Figure 1.

A. Overview of PBT Model

The PBT channel model considers a wireless communication link between a transmitter equipped with a unipolarized continuous linear array of length $2L_T$ and a receiver with a similar array of length $2L_R$. The authors observe that there are two key domains: the *array domain*, which describes the current distribution on the arrays, and the *wavevector domain* which describes the field patterns. Assume the physical objects that scatter the fields radiated from the transmit array to the receive array subtend an angle Θ_T at the transmit array an angle Θ_R at the receive array. Because a linear array aligned to the z-axis array can only resolve the z-component, i.e. the $\cos\theta$ component, consider the sets $\Psi_T = \{\cos\theta : \theta \in \Theta_T\}$ and $\Psi_R = \{\cos\theta : \theta \in \Theta_R\}$. In [7], it is shown from the first principles of Maxwell's equations that an array of length $2L_T$ has a resolution of $1/(2L_T)$ over the interval Ψ_T, so that the dimension of the transmit signal space of radiated field patterns is $2L_T|\Psi_T|$. Likewise the dimension of the receive signal space is $2L_R|\Psi_R|$, so that the degrees of freedom of the communication link is

$$d_{\text{P2P}} = \min\left\{2L_T|\Psi_T|, 2L_R|\Psi_R|\right\}. \tag{1}$$

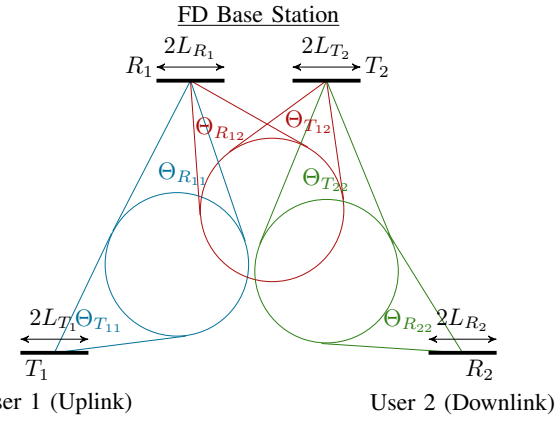

Fig. 2: Clustered scattering. Only one cluster for each transmit receive pair is shown to prevent clutter.

B. Extension of PBT Model to Three-Node Full-Duplex

Figure 2 illustrates our extension of the PBT channel model to the three-node full-duplex topology of Figure 1. Let Flow_1 denote the uplink flow from User 1 to the base station, and Flow_2 denote the downlink flow from the base station to User 2. Let T_1 and R_1 denote the transmitter and receiver for Flow_1, respectively, and T_2 and R_2 denote the the transmitter and receiver for Flow_2. Each of the two transmitters $T_j,\ j = 1, 2$ is equipped with a linear array of length $2L_{T_j}$, and each receiver, $R_i,\ i = 1, 2$ is equipped a linear array of length $2L_{R_i}$.

1) Scattering Intervals: Let $\theta_{T_j} \in [0, \pi]$ denote the elevation angle relative to the T_j and let θ_{R_i} denote the elevation angle relative to the R_i array. As depicted in Figure 2, $\Theta_{T_{ij}}$ denotes the angular spread subtended at transmitter T_j by the physical objects that scatter fields radiated from T_j to R_i. Similarly let $\Theta_{R_{ij}}$ denote the corresponding angular spread subtended at R_i by scatterers illuminated by T_j. Thus, we see in Figure 2 that from the point-of-view of the base-station transmitter, T_2, $\Theta_{T_{22}}$ is the angular interval over which it can radiate signals that will couple to its intended receiver, while $\Theta_{T_{12}}$ is the interval in which the radiated signal will bounce back to the base station receiver, R_1, as self-interference. We assume that the user devices are hidden from each other such that $\Theta_{T_{21}} = \Theta_{R_{21}} = \emptyset$. In Figure 2, the six scattering intervals are drawn as being circular and angularly contiguous, but this is purely for the sake of making the figure uncluttered, and need not be the case. Because linear arrays can only resolve the cosine of the elevation angle, let $t_j \equiv \cos\theta_{T_j} \in [-1, 1]$, and likewise $\tau_i \equiv \cos\theta_{R_i} \in [-1, 1]$. Denote the "effective" scattering interval as

$$\Psi_{T_{ij}} \equiv \left\{t_j : \arccos(t_j) \in \Theta_{T_{ij}}\right\} \subset [-1, 1].$$

Likewise for the receiver side we denote the effective scattering intervals as

$$\Psi_{R_{ij}} \equiv \left\{\tau_i : \arccos(\tau_i) \in \Theta_{R_{ij}}\right\} \subset [-1, 1].$$

Define the width of the transmit and receive scattering intervals as $|\Psi_{T_{ij}}| = \int_{\Psi_{T_{ij}}} dt_j$ and $|\Psi_{R_{ij}}| = \int_{\Psi_{R_{ij}}} d\tau_i$, respectively.

2) Hilbert space channel model: Let $\mathcal{T}_j$ be the Hilbert space of all square integrable transmit field distributions $X_j : \Psi_{T_{jj}} \cup \Psi_{T_{ij}} \to \mathbb{C}$ that transmitter T_j's array of length L_{T_j} can radiate in the direction of the available scattering clusters. The inner product between two member functions, $U_j, V_j \in \mathcal{T}_j$, is the usual inner product $\langle U_j, V_j\rangle = \int_{\Psi_{T_{jj}} \cup \Psi_{T_{ij}}} U_j(t)V_j^*(t)\,dt$. Likewise let $\mathcal{R}_i$ the Hilbert space of all received field distributions $Y_i : \Psi_{R_{ii}} \cup \Psi_{R_{ij}} \to \mathbb{C}$ incident on receiver R_i and resolved by an array of length L_{R_i}. From [7], we know that the dimension of these transmit and receive signal spaces are, respectively,

$$\dim \mathcal{T}_j = 2L_{T_j}|\Psi_{T_{jj}} \cup \Psi_{T_{ij}}|, \tag{2}$$
$$\dim \mathcal{R}_i = 2L_{R_i}|\Psi_{R_{ii}} \cup \Psi_{R_{ij}}|. \tag{3}$$

Define the channel scattering operator $\mathsf{H}_{ij} : \mathcal{T}_j \to \mathcal{R}_i$ by

$$(\mathsf{H}_{ij}X_j)(\tau) = \int_{\Psi_{T_{ij}} \cup \Psi_{T_{jj}}} H_{ij}(\tau, t)X_j(t)\,dt,\ \ \tau \in \Psi_{R_{ij}} \cup \Psi_{R_{ii}}. \tag{4}$$

With the above definitions, we write the channel input-output relationship

$$Y_1 = \mathsf{H}_{11}X_1 + \mathsf{H}_{12}X_2 + Z_1, \tag{5}$$
$$Y_2 = \mathsf{H}_{22}X_2 + Z_2, \tag{6}$$

where $X_j \in \mathcal{T}_j$ is the wavevector signal transmitted by T_j, $Y_i \in \mathcal{R}_i$ is the wavevector signal received by R_i and $Z_i \in \mathcal{R}_i$ is additive noise. The impact of the scattering intervals is captured in the behavior of the scattering response integral kernel $H_{ij}(\tau, t)$, which we endow with the properties:

1) $H_{ij}(\tau,t) \neq 0$ only if $(\tau,t) \in \Psi_{R_{ij}} \times \Psi_{T_{ij}}$,
2) $\int ||H_{ij}(\tau,t)||dt \neq 0 \ \forall \ \tau \in \Psi_{R_{ij}}$,
3) $\int ||H_{ij}(\tau,t)||d\tau \neq 0 \ \forall \ t \in \Psi_{T_{ij}}$,
4) The point spectrum of $H_{ij}(\cdot,\cdot)$ is infinite.

Let $R(\mathsf{H}_{ij}) \subset \mathcal{R}_i$ denote the range of scattering operator H_{ij}, and let $R(\mathsf{H}_{ij})^\perp \subset \mathcal{R}_i$ denote the orthogonal complement of $R(\mathsf{H}_{ij})$. Let $N(\mathsf{H}_{ij}) \subset \mathcal{T}_j$ denote the nullspace of H_{ij}, and $N(\mathsf{H}_{ij})^\perp$ its orthogonal space (i.e. the coimage of H_{ij}). The results of [7] can be combined with standard theorems of functional analysis to show the following properties:

$$\begin{aligned}\dim R(\mathsf{H}_{ij}) &= \dim N(\mathsf{H}_{ij})^\perp \\ &= 2\min\{L_{T_j}|\Psi_{T_{ij}}|, L_{R_i}|\Psi_{R_{ij}}|\}, \quad (7)\\ \dim N(\mathsf{H}_{12}) &= 2L_{T_2}|\Psi_{T_{22}} \setminus \Psi_{T_{12}}| \\ &\quad + 2(L_{T_2}|\Psi_{T_{12}}| - L_{R_1}|\Psi_{R_{12}}|)^+, \quad (8)\\ \dim R(\mathsf{H}_{11})^\perp &= 2L_{R_1}|\Psi_{T_{12}} \setminus \Psi_{T_{11}}| \\ &\quad + 2(L_{R_1}|\Psi_{R_{11}}| - L_{T_1}|\Psi_{T_{11}}|)^+. \quad (9)\end{aligned}$$

III. Degrees-of-Freedom Analysis

Theorem 1: Let d_1 and d_2 be the degrees of freedom of Flow_1 and Flow_2 respectively. The degrees-of-freedom region, $\mathcal{D}_{\mathsf{FD}}$, of the three-node full-duplex channel is the convex hull of the degrees-of-freedom pairs, (d_1, d_2), satisfying

$$\begin{aligned}d_1 \leq d_1^{\max} &= 2\min(L_{T_1}|\Psi_{T_{11}}|, L_{R_1}|\Psi_{R_{11}}|), \quad (10)\\ d_2 \leq d_2^{\max} &= 2\min(L_{T_2}|\Psi_{T_{22}}|, L_{R_2}|\Psi_{R_{22}}|), \quad (11)\\ d_1 + d_2 \leq d_{\mathsf{sum}}^{\max} &= 2L_{T_2}|\Psi_{T_{22}} \setminus \Psi_{T_{12}}| + 2L_{R_1}|\Psi_{R_{11}} \setminus \Psi_{R_{12}}| \\ &\quad + 2\max(L_{T_2}|\Psi_{T_{12}}|, L_{R_1}|\Psi_{R_{12}}|). \quad (12)\end{aligned}$$

The degrees-of-freedom region, $\mathcal{D}_{\mathsf{FD}}$, is depicted in Figure 3. The achievability part of Theorem 1 is given in Section III-A and a sketch of the converse is given in Section III-B.

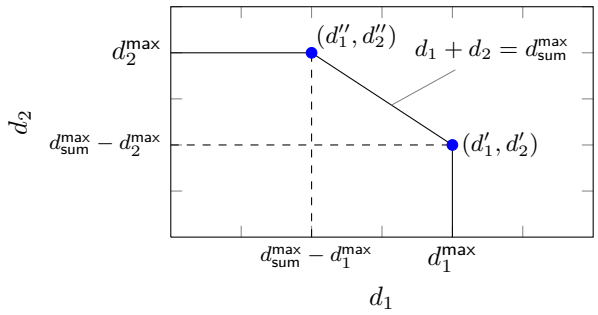

Fig. 3: degrees-of-freedom region, $\mathcal{D}_{\mathsf{FD}}$

A. Achievability

We establish achievability of $\mathcal{D}_{\mathsf{FD}}$ by way of two lemmas. The first lemma shows the achievability of two specific degree-of-freedom pairs, and the second lemma remarks that these pairs are the corner points of $\mathcal{D}_{\mathsf{FD}}$.

Lemma 1: The degree-of-freedom pairs (d_1', d_2') and (d_1'', d_2'') are achievable, where

$$\begin{aligned}d_1' &= \min\{2L_{T_1}|\Psi_{T_{11}}|, 2L_{R_1}|\Psi_{R_{11}}|\}, \quad (13)\\ d_2' &= \min\{d_{T_2}, 2L_{R_2}|\Psi_{R_{22}}|\}\,1(L_{T_1}|\Psi_{T_{11}}| \geq L_{R_1}|\Psi_{R_{11}}|) \\ &\quad + \min\{\delta_{T_2}, 2L_{R_2}|\Psi_{R_{22}}|\}\,1(L_{T_1}|\Psi_{T_{11}}| < L_{R_1}|\Psi_{R_{11}}|), \quad (14)\\ d_1'' &= \min\{2L_{T_1}|\Psi_{T_{11}}|, d_{R_1}\}\,1(L_{R_2}|\Psi_{R_{22}}| \geq L_{T_2}|\Psi_{T_{22}}|) \\ &\quad + \min\{2L_{T_1}|\Psi_{T_{11}}|, \delta_{R_1}\}\,1(L_{R_2}|\Psi_{R_{22}}| < L_{T_2}|\Psi_{T_{22}}|), \quad (15)\\ d_2'' &= \min\{2L_{T_2}|\Psi_{T_{22}}|, 2L_{R_2}|\Psi_{R_{22}}|\}, \quad (16)\end{aligned}$$

with d_{T_2},δ_{T_2}, d_{R_1}, and δ_{R_1} given in (17-20) at the top of the following page.

Sketch of Proof: The proof is inspired by the zero-forcing scheme of [10] for the MIMO interference channel, except that processing is performed in continuous Hilbert spaces rather than discrete vector spaces, and the fact that scattering intervals are not perfectly overlapped requires some extra treatment. The full proof is omitted for brevity, but sketch the achievability of (d_1', d_2') when $L_{T_1}|\Psi_{T_{11}}| \geq L_{R_1}|\Psi_{R_{11}}|$, $d_{T_2} \leq 2L_{R_2}|\Psi_{R_{22}}|$, $L_{T_2}|\Psi_{T_{22}} \cap \Psi_{T_{12}}| \geq 2(L_{T_2}|\Psi_{T_{12}}| - L_{R_1}|\Psi_{R_{12}}|)^+ + 2L_{R_1}|\Psi_{R_{12}} \setminus \Psi_{R_{11}}|$, and $L_{T_2}|\Psi_{T_{12}}| \geq L_{R_1}|\Psi_{R_{12}}|$. In this case (13) and (14) simplify to

$$\begin{aligned}d_1' &= 2L_{R_1}|\Psi_{R_{11}}|, \quad (21)\\ d_2' &= 2(L_{T_2}|\Psi_{T_{22}} \setminus \Psi_{T_{12}}| + (L_{T_2}|\Psi_{T_{12}}| - L_{R_1}|\Psi_{R_{12}}|) \\ &\quad + L_{R_1}|\Psi_{R_{12}} \setminus \Psi_{R_{11}}|). \quad (22)\end{aligned}$$

We give Flow_1 its maximum point-to-point degrees of freedom, which is shown in [7] to be $\min\{2L_{T_1}|\Psi_{T_{11}}, 2L_{R_1}|\Psi_{R_{11}}|\} = 2L_{R_1}|\Psi_{R_{11}}| = d_1'$. The wavevector received at R_1 from T_1, $\mathsf{H}_{11}X_1$, necessarily lies in $R(\mathsf{H}_{11})$. If T_2 can construct its transmitted wavevector signal, X_2, such that $\mathsf{H}_{12}X_2 \in R(\mathsf{H}_{11})^\perp$ then we will have $\mathsf{H}_{11}X_1 \perp \mathsf{H}_{12}X_2$ and thus T_2 will not impede R_1's recovery of the d_1' symbols from T_1. Let $\mathcal{P}_{12} \equiv \mathsf{H}_{12}{}^{\leftarrow}(R(\mathsf{H}_{11})^\perp) \subseteq \mathcal{T}_2$ denote the preimage of $R(\mathsf{H}_{11})^\perp$ under H_{12}. Then constructing X_2 such that $X_2 \in \mathcal{P}_{12}$ ensures $\mathsf{H}_{11}X_1 \perp \mathsf{H}_{12}X_2$. Since we are considering the case where $L_{T_2}|\Psi_{T_{12}}| \geq L_{R_1}|\Psi_{R_{12}}|$, $R(\mathsf{H}_{11})^\perp \subseteq R(\mathsf{H}_{12})$ and thus

$$\begin{aligned}\dim \mathcal{P}_{12} &= \dim N(\mathsf{H}_{12}) + \dim R(\mathsf{H}_{11})^\perp \quad (23)\\ &= 2(L_{T_2}|\Psi_{T_{22}} \setminus \Psi_{T_{12}}| + (L_{T_2}|\Psi_{T_{12}}| - L_{R_1}|\Psi_{R_{12}}|) \\ &\quad + L_{R_1}|\Psi_{R_{12}} \setminus \Psi_{R_{11}}|) \quad (24)\\ &= d_2', \quad (25)\end{aligned}$$

where in (24) we have leveraged properties (8) and (9) from Section II. Therfore T_2 can transmit the required d_2' symbols along each basis function of any orthonormal basis of $\mathcal{P}_{12}$,

$$d_{T_2} = 2L_{T_2}|\Psi_{T_{22}} \setminus \Psi_{T_{12}}| + 2\min\left\{L_{T_2}|\Psi_{T_{22}} \cap \Psi_{T_{12}}|, (L_{T_2}|\Psi_{T_{12}}| - L_{R_1}|\Psi_{R_{12}}|)^+ + L_{R_1}|\Psi_{R_{12}} \setminus \Psi_{R_{11}}|\right\}^+ \quad (17)$$

$$\delta_{T_2} = 2L_{T_2}|\Psi_{T_{22}} \setminus \Psi_{T_{12}}| + 2\min\left\{L_{T_2}|\Psi_{T_{22}\cap\Psi_{T_{12}}}|,\ L_{T_2}|\Psi_{T_{12}}| - \left[L_{T_1}|\Psi_{T_{11}}| - \left(L_{R_1}|\Psi_{R_{11}\setminus\Psi_{R_{12}}}| + (L_{R_2}|\Psi_{R_{12}}| - L_{T_1}|\Psi_{T_{12}}|)^+\right)\right]^+\right\} \quad (18)$$

$$d_{R_1} = 2L_{R_1}|\Psi_{R_{11}} \setminus \Psi_{R_{12}}| + 2\min\left\{L_{R_1}|\Psi_{R_{11}} \cap \Psi_{R_{12}}|, (L_{R_1}|\Psi_{R_{12}}| - L_{T_2}|\Psi_{T_{12}}|)^+ + L_{T_2}|\Psi_{T_{12}} \setminus \Psi_{T_{22}}|\right\}^+ \quad (19)$$

$$\delta_{R_1} = 2L_{R_1}|\Psi_{R_{11}} \setminus \Psi_{R_{12}}| + 2\min\left\{L_{R_1}|\Omega_{R_{11}\cap\Psi_{R_{12}}}|,\ L_{R_1}|\Psi_{R_{12}}| - \left[L_{R_2}|\Psi_{R_{22}}| - \left(L_{T_2}|\Psi_{T_{22}\setminus\Psi_{T_{12}}}| + (L_{T_2}|\Psi_{T_{12}}| - L_{R_1}|\Psi_{R_{12}}|)^+\right)\right]^+\right\} \quad (20)$$

thus avoiding interfering R_1. And since in the case we are considering d_2' is no larger than $\min\{2L_{T_2}|\Psi_{T_{22}}|, 2L_{R_2}|\Psi_{R_{22}}|\}$, which is the number of degrees of freedom Flow_2 can support, R_2 can recover the d_2' of the symbols transmitted from T_2, as desired.

■

Lemma 2: The degree-of-freedom pairs (d_1', d_2') and (d_1'', d_2''), are the corner points of $\mathcal{D}_{\mathsf{FD}}$.

Sketch of Proof: One can check that

$$(d_1', d_2') = (d_1^{\mathsf{max}}, d_{\mathsf{FD}}^{\mathsf{sum}} - d_1^{\mathsf{max}}) \quad (26)$$

$$(d_1'', d_2'') = (d_{\mathsf{FD}}^{\mathsf{sum}} - d_2^{\mathsf{max}}, d_2^{\mathsf{max}}). \quad (27)$$

by exhausting computing the left and right and sides of (26) and (27) in all cases and observing equality. We omit the computations for brevity. ■

Lemmas 1 and 2 show that the corner points of $\mathcal{D}_{\mathsf{FD}}$, (d_1', d_2') and (d_1'', d_2'') are achievable. And thus all other points within $\mathcal{D}_{\mathsf{FD}}$ are achievable via time sharing between the schemes that achieve the corner points.

B. Converse

The full converse is omitted, for brevity, but here we give a sketch the procedure for showing the converse part of Theorem 1. We would like to show that if the degree-of-freedom pair (d_1, d_2) is achievable, then $(d_1, d_2) \in \mathcal{D}_{\mathsf{FD}}$. It is easy to see that if (d_1, d_2) is achievable, then constraints (10) and (11) must be satisfied as these are the point-to-point bounds given in [7]. It remains to show that the sum degree-of-freedom constrain (12) must hold for every achievable (d_1, d_2). Our process for showing (12) is twofold.

First, a genie expands the scattering intervals $\Psi_{T_{22}}$ and $\Psi_{T_{12}}$, to $\Psi'_{T_{22}} = \Psi'_{T_{12}} = \Psi_{T_{22}} \cup \Psi_{T_{12}}$, and also expands $\Psi_{R_{11}}$ and $\Psi_{R_{12}}$ to $\Psi'_{R_{11}} = \Psi'_{R_{12}} = \Psi_{R_{11}} \cup \Psi_{R_{12}}$. The genie also lengthens the T_2 array to $L'_{T_2} = L_{T_2} + L_{R_1}\frac{|\Psi_{R_{11}}\setminus\Psi_{R_{12}}|}{|\Psi_{T_{22}}\cup\Psi_{T_{12}}|}$ and the R_1 array to length $L'_{R_1} = L_{R_1} + L_{T_2}\frac{|\Psi_{T_{22}}\setminus\Psi_{T_{12}}|}{|\Psi_{R_{11}}\cup\Psi_{R_{12}}|}$, which one can show ensures that any added interference due to the expansion of $\Psi_{T_{12}}$ and $\Psi_{R_{12}}$ is compensated by the larger arrays sizes so that the net manipulation of the genie can only enlarge $\mathcal{D}_{\mathsf{FD}}$.

One can check that after above genie manipulation is performed, the maximum of the T_2 and R_1 signaling dimensions are equal to $d_{\mathsf{sum}}^{\mathsf{max}}$ in constraint (12), and since the scattering intervals are overlapped, the channel model becomes the Hilbert space equivalent of the well-studied MIMO Z-channel. The Hilbert space analog to the bounding techniques employed in [10], [11] that show the sum degrees of freedom of the MIMO z-channel is bound by $\max(M_2, N_1)$ can be leveraged to show (12) as desired.

IV. Impact on Full-duplex Design

Let $\mathcal{D}_{\mathsf{HD}}$ be the region of degree-of-freedom pairs achievable via half-duplex mode, i.e. by time-division-duplex between transmission at T_1 and T_2, so that there is no self-interference in this case. It is easy to see that the half-duplex achievable region is characterized by

$$d_1 \le \alpha \min\{2L_{T_1}|\Psi_{T_{11}}|, 2L_{R_1}|\Psi_{R_{11}}|\}, \quad (28)$$

$$d_2 \le (1-\alpha)\min\{2L_{T_2}|\Psi_{T_{22}}|, 2L_{R_2}|\Psi_{R_{22}}|\}, \quad (29)$$

where $\alpha \in [0,1]$ is the time sharing parameter. Obviously $\mathcal{D}_{\mathsf{HD}} \subseteq \mathcal{D}_{\mathsf{FD}}$, but we are interested in contrasting the scenarios for which $\mathcal{D}_{\mathsf{HD}} \subset \mathcal{D}_{\mathsf{FD}}$, and full-duplex spatial isolation strictly outperforms half-duplex time division, and the scenarios for which $\mathcal{D}_{\mathsf{HD}} = \mathcal{D}_{\mathsf{FD}}$ and half-duplex can achieve the same performance as full-duplex. We will consider two particularly interesting cases: the fully spread environment, and the symmetric spread environment.

A. Fully Spread

Consider case where the environment is fully spread,

$$|\Psi_{T_{11}}| = |\Psi_{R_{11}}| = |\Psi_{T_{22}}| = |\Psi_{R_{22}}| = |\Psi_{T_{12}}| = |\Psi_{R_{12}}| = 2.$$

For simplicity also assume that the base station transmit and receive arrays are of length $L_{R_1} = L_{T_2} = L_{\mathsf{BS}}$, and user arrays are of length $L_{T_1} = L_{R_2} = L_{\mathsf{Usr}}$. In this case the full-duplex degree-of-freedom region, $\mathcal{D}_{\mathsf{FD}}$, simplifies to

$$d_i \le 4\min\{L_{\mathsf{BS}}, L_{\mathsf{Usr}}\}, i = 1, 2; \quad d_1 + d_2 \le 4L_{\mathsf{BS}} \quad (30)$$

while the half-duplex achievable region, $\mathcal{D}_{\mathsf{HD}}$ simplifies to

$$d_1 + d_2 \le 4\min\{L_{\mathsf{BS}}, L_{\mathsf{Usr}}\}. \quad (31)$$

Remark: In the fully-scattered case, $\mathcal{D}_{\mathsf{HD}} \subset \mathcal{D}_{\mathsf{FD}}$ if $L_{\mathsf{BS}} > L_{\mathsf{Usr}}$, else $\mathcal{D}_{\mathsf{HD}} = \mathcal{D}_{\mathsf{FD}}$.

B. Symmetric Spread

We will consider a special case that illustrates the impact of the overlap of the scattering intervals on full-duplex performance. Assume all the arrays in the network, the two arrays on the base station as well as the array on each of the user devices, are of the same length L, that is $L_{T_1} = L_{R_1} = L_{T_2} = L_{R_2} = L$. Assume also the size of the scattering interval to/from the intended receiver/transmitter is the same for all arrays $|\Psi_{T_{11}}| = |\Psi_{R_{11}}| = |\Psi_{T_{22}}| = |\Psi_{R_{22}}| = |\Psi_{\mathsf{Fwd}}|$. Finally assume that $|\Psi_{T_{12}}| = |\Psi_{R_{12}}| = |\Psi_{\mathsf{Back}}|$, and that the amount of overlap with the intended-signal scattering interval is the same so that $|\Psi_{T_{22}} \cap \Psi_{T_{12}}| = |\Psi_{R_{11}} \cap \Psi_{R_{12}}| = |\Psi_{\mathsf{Fwd}} \cap \Psi_{\mathsf{Back}}| = |\Psi_{\mathsf{Fwd}}| - |\Psi_{\mathsf{Fwd}} \setminus \Psi_{\mathsf{Back}}|$.

We call Ψ_{Back} the *backscatter interval* since it is the angle subtended at the base station by the back-scattering clusters, while we call Ψ_{Fwd} the *forward interval*, since it is the angle subtended by the clusters that scatter towards the intended transmitter/receiver. In this symmetric case, the full-duplex degree-of-freedom region, $\mathcal{D}_{\mathsf{FD}}$ simplifies to

$$d_i \leq 2L|\Psi_{\mathsf{Fwd}}|, \ i = 1, 2 \tag{32}$$

$$d_1 + d_2 \leq 2L(2|\Psi_{\mathsf{Fwd}} \setminus \Psi_{\mathsf{Back}}| + |\Psi_{\mathsf{Back}}|) \tag{33}$$

while the half-duplex achievable region, $\mathcal{D}_{\mathsf{HD}}$ is

$$d_1 + d_2 \leq 2L|\Psi_{\mathsf{Fwd}}|. \tag{34}$$

Remark: Comparing $\mathcal{D}_{\mathsf{FD}}$ and $\mathcal{D}_{\mathsf{HD}}$ above we see that in the case of symmetric scattering, $\mathcal{D}_{\mathsf{HD}} = \mathcal{D}_{\mathsf{FD}}$ if and only if $\Psi_{\mathsf{Fwd}} = \Psi_{\mathsf{Back}}$,[1] else $\mathcal{D}_{\mathsf{HD}} \subset \mathcal{D}_{\mathsf{FD}}$.
Thus the full-duplex spatial isolation region is strictly larger than the half-duplex time-division region unless the forward interval and the backscattering interval are exactly aligned. The intuition is that when $\Psi_{\mathsf{Fwd}} = \Psi_{\mathsf{Back}}$ the scattering interval must be shared, just as time must be, thus trading spatial resources is equivalent to trading time-slots. However, if $\Psi_{\mathsf{Fwd}} \neq \Psi_{\mathsf{Back}}$, there is a portion of space exclusive to each user, and can be leveraged to improve upon time division.

Remark: In the case of symmetric scattering, the full-duplex degree-of-freedom region is rectangular if and only if

$$|\Psi_{\mathsf{Back}} \setminus \Psi_{\mathsf{Fwd}}| \geq |\Psi_{\mathsf{Fwd}} \cap \Psi_{\mathsf{Back}}|. \tag{35}$$

The above remark can be verified by comparing (32) and (33) observing that the sum-rate bound, (33), is only active when

$$2|\Psi_{\mathsf{Fwd}} \setminus \Psi_{\mathsf{Back}}| + |\Psi_{\mathsf{Back}}| \geq 2|\Psi_{\mathsf{Fwd}}|. \tag{36}$$

A few lines of set-algebraic manipulation of condition (36) shows that it is equivalent to (35). One intuition behind this remark is that when $|\Psi_{\mathsf{Back}} \setminus \Psi_{\mathsf{Fwd}}| \geq |\Psi_{\mathsf{Fwd}} \cap \Psi_{\mathsf{Back}}|$, then the interval $|\Psi_{\mathsf{Fwd}} \cap \Psi_{\mathsf{Back}}|$ can be used as interference free side-channel on which it can communicate the interference it is generating over $|\Psi_{\mathsf{Fwd}} \cap \Psi_{\mathsf{Back}}|$, so that the interference can be cancelled.

Consider the case where $|\Psi_{\mathsf{Fwd}}| = 1$ and $|\Psi_{\mathsf{Back}}| = 1$, thus the overlap between the two, $|\Psi_{\mathsf{Fwd}} \cap \Psi_{\mathsf{Back}}|$ can vary from zero to one. Figure 4 plots the half-duplex region, $\mathcal{D}_{\mathsf{HD}}$, and the full-duplex region, $\mathcal{D}_{\mathsf{FD}}$, for several different values of overlap, $|\Psi_{\mathsf{Fwd}} \cap \Psi_{\mathsf{Back}}|$. We see that when $\Psi_{\mathsf{Fwd}} = \Psi_{\mathsf{Back}}$ so that $|\Psi_{\mathsf{Fwd}} \cap \Psi_{\mathsf{Back}}| = 1$, both $\mathcal{D}_{\mathsf{HD}}$ and $\mathcal{D}_{\mathsf{FD}}$ are the same triangular region. When $|\Psi_{\mathsf{Fwd}} \cap \Psi_{\mathsf{Back}}| = 0.75$, we get a rectangular region. Once $|\Psi_{\mathsf{Fwd}} \cap \Psi_{\mathsf{Back}}| \leq 0.5$, $|\Psi_{\mathsf{Back}} \setminus \Psi_{\mathsf{Fwd}}|$ becomes greater than 0.5, such that condition of (35) is satisfied and the degree-of-freedom region becomes rectangular.

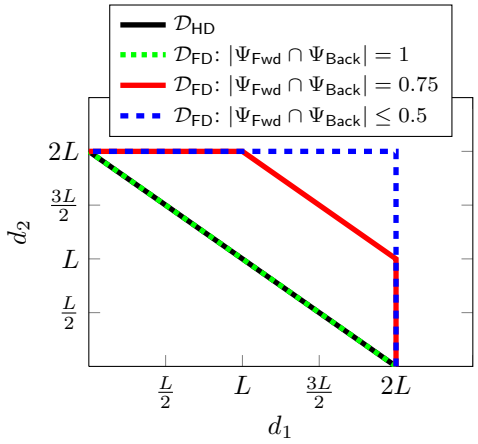

Fig. 4: Symmetric-spread degree-of-freedom regions for different amounts of scattering overlap

[1] We are neglecting the trivial case of $L = 0$.

References

[1] M. Duarte, C. Dick, and A. Sabharwal, "Experiment-driven characterization of full-duplex wireless systems," *Wireless Communications, IEEE Transactions on*, vol. 11, no. 12, pp. 4296–4307, 2012.

[2] A. Sahai, G. Patel, C. Dick, and A. Sabharwal, "On the impact of phase noise on active cancelation in wireless full-duplex," *Vehicular Technology, IEEE Transactions on*, vol. 62, no. 9, pp. 4494–4510, 2013.

[3] D. W. Bliss, P. A. Parker, and A. R. Margetts, "Simultaneous transmission and reception for improved wireless network performance," in *Proceedings of the 2007 IEEE/SP 14th Workshop on Statistical Signal Processing*. Washington, DC, USA: IEEE Computer Society, 2007, pp. 478–482.

[4] B. Day, A. Margetts, D. Bliss, and P. Schniter, "Full-duplex bidirectional MIMO: Achievable rates under limited dynamic range," *Signal Processing, IEEE Transactions on*, vol. 60, no. 7, pp. 3702 –3713, july 2012.

[5] E. Everett, M. Duarte, C. Dick, and A. Sabharwal, "Empowering full-duplex wireless communication by exploiting directional diversity," in *Asilomar Conference on Signals, Systems and Computers*, October 2011.

[6] E. Everett, A. Sahai, and A. Sabharwal, "Passive self-interference suppression for full-duplex infrastructure nodes," *Wireless Communications, IEEE Transactions on*, to be published. [Online]. Available: http://arxiv.org/abs/1302.2185

[7] A. Poon, R. Brodersen, and D. Tse, "Degrees of freedom in multiple-antenna channels: a signal space approach," *Information Theory, IEEE Transactions on*, vol. 51, no. 2, pp. 523 – 536, feb. 2005.

[8] A. Poon, D. Tse, and R. Brodersen, "Impact of scattering on the capacity, diversity, and propagation range of multiple-antenna channels," *Information Theory, IEEE Transactions on*, vol. 52, no. 3, pp. 1087 – 1100, march 2006.

[9] A. Poon and D. Tse, "Degree-of-freedom gain from using polarimetric antenna elements," *Information Theory, IEEE Transactions on*, vol. 57, no. 9, pp. 5695 –5709, sept. 2011.

[10] S. Jafar and M. Fakhereddin, "Degrees of freedom for the mimo interference channel," *Information Theory, IEEE Transactions on*, vol. 53, no. 7, pp. 2637–2642, 2007.

[11] L. Ke and Z. Wang, "Degrees of freedom regions of two-user mimo z and full interference channels: The benefit of reconfigurable antennas," *Information Theory, IEEE Transactions on*, vol. 58, no. 6, pp. 3766–3779, 2012.